First-order type A waveguide Bragg gratings with under-diffraction-limited periodicities and sub-millimeter length for NIR applications

Laura Loi, Mathis Carpentier, Yannick Petit, Lionel Canioni

Research Article Vol. 14, No. 7 / 1 Jul 2024 / Optical Materials Express 1837
Optical Materials EXPRESS

First-order type A waveguide Bragg gratings with under-diffraction-limited periodicities and sub-millimeter length for NIR applications

Laura Loi,[1] Mathis Carpentier,[2] Yannick Petit,[1,2,*] and Lionel Canioni[1,2]

[1] Université de Bordeaux, CNRS, CEA, CELIA, UMR 5107, F-33405 Talence, France
[2] Université de Bordeaux, CNRS, INP, ICMCB, UMR 5026, F-33600 Pessac, France
[*] yannick.petit@u-bordeaux.fr

Abstract: Since its demonstration in 2017, laser-induced Type A modifications in silver-containing glasses have been exploited for fabricating waveguides, couplers, volume Bragg Gratings and, more recently, waveguides Bragg Gratings. Laser-induced silver-supported structures exhibit sub-diffraction characteristics being always associated with a positive refractive index change resulting from multi-photon energy deposition under multiple-pulse femtosecond laser irradiation. These properties have been exploited in this work for the fabrication of efficient first-order helicoidal Type A waveguides Bragg gratings in the near-infrared (NIR) range, with periodicities well below the diffraction limit and with typical length $L = 500$ μm, showing narrowband mirror behaviours. Moreover, this work demonstrates that such helicoidal Type A waveguides Bragg gratings allow for modulating the refractive index of the waveguide at half the periodicity of the helix. Such a peculiarity has been exploited to fabricate efficient first-order Type A waveguides Bragg gratings in the NIR range, as well as in the far red range of the visible spectrum, showing a remarkably strong coupling coefficient, up to one order of magnitude higher than what is reported in the literature.

1. Introduction

Waveguides Bragg Gratings (WBGs) are optical devices obtained by periodically modulating the refractive index of the waveguide to fabricate 1D photonic bandgap. Conceptually similar to Fiber Bragg Gratings (FBGs), WBGs act as narrowband mirrors at specific wavelengths λ_B, which are selected by the period of the refractive index perturbation Λ_G, the mean effective refractive index n_{eff} of the guided mode over a period, and the order m of the diffraction:[1]

$$\lambda_B = \frac{2\, n_{eff}\, \Lambda_G}{m}. \tag{1}$$

WBGs, as well as FBGs, can be used for wavelength division multiplexing (WDM) and therefore can find several applications in a wide range of fields: for instance, chirped WBGs can provide dispersion compensation in optical communications laser systems, while phase-shifted gratings find applications in temporal differentiation and filtering. Most commonly, the modulation of the refractive index of the guiding structure is achieved in photosensitive media by holographic interferometry of UV light, or by adopting a phase-mask approach [2–6]. As for the latter, long and efficient gratings can be obtained by UV or IR radiations for which a single phase-mask allows for the inscription of only one pre-determined grating period. Therefore, such a fabrication process is not versatile, since different masks are required to obtain different periodicities. On the other hand, BGs have also been inscribed for more than a decade in the bulk of media by Femtosecond Laser Inscription (FLI) [7–14]. This fabrication method is based on multiphoton absorption, a nonlinear process induced only in the interaction voxel

#519762 https://doi.org/10.1364/OME.519762
Journal © 2024 Received 22 Jan 2024; revised 19 Apr 2024; accepted 1 May 2024; published 12 Jun 2024

Optical Materials EXPRESS

of a focused femtosecond laser source. As a result, the FLI allows for directly addressing 3D material structuring in a strongly-confined voxel. In the case of glassy media, femtosecond interaction induced rearrangements of the glass matrix such as densification and the creation of color centers from which three types of refractive index change arise depending on the laser fluence [15–18]. At low fluence, Type I modifications are associated with a smooth refractive index change, while higher laser fluence can lead to the formation of nanogratings, labelled as Type II modifications, which are characterized by birefringent effects. Finally, at high laser fluence micro-voids, characterized by a strong index contrast, are obtained and classified as Type III modifications. In the fabrication of FBGs and WBGs, Type II modifications can be used to control the Bragg resonances of orthogonally polarized modes, while Type III modifications are exploited in photonics bandgap devices [13,14]. Still, Type I is generally preferred in integrated optics as it limits laser-induced losses compared to Type II and Type III. Beyond these commonly considered types of modifications, another type of refractive index change was introduced in 2017 and investigated in silver-containing glasses, namely Type A standing for *argentum*. This positive index contrast arises from the photochemistry of silver ions induced by the interaction of the femtosecond laser and the glass matrix. The silver-sustained inscribed structures show features overcoming the diffraction limit and re-writing ability, which allows for fabricating periodic structures with sub-wavelength periodicity in glass compositions where silver ions had been inserted and well isolated either during the melting process [19–24] or thanks to silver ion exchange after the quenching step [25]. Most of the demonstrations were led in oxide glasses [19–25] but oxifluoride glasses are also promising candidates [26,27]. In particular, these properties have been exploited in the work of Laberdesque *et al.*, demonstrating the fabrication of the firsts efficient first-order WBGs sustained by Type A refractive index modifications which targeted the Visible-Near-Infrared (VIS-NIR) range, with achieved periodicities down to 240 nm [23].

The universal development of this technique of efficient first-order WBGs sustained by Type A refractive index modifications requires to access the following needs : (i) the considered glass matrix need to allow for the sufficient insertion of well-dispersed silver ions (up to a few molar percents); (ii) the UV cut-off of the glass matrix needs to be at similar or ideally at smaller wavelength than the absorption bands of well dispersed silver ions; (iii) the pristine glass should ideally have sufficiently oxidative properties to prevent from the spontaneous formation of silver clusters or of metallic silver nanoparticles; and (iv) under laser irradiation, the glass matrix should have sufficient charge compensators (such as non-bridging oxygens) to allow for a good mobility of silver species so as to create and grow molecular silver clusters with associated highly-localized sub-micron refractive index modulation while preventing massive silver metallic nanoparticles that tend to produce much less localized features which is detrimental for the achievement of sub-micron periodicities for the production of WBGs. The optimization of this Type A approach of WBG inscription relies thus on a subtle balance between the glass matrix behavior and the laser/glass irradiation parameters.

In this framework, the work reported in this article validates the results achieved by Laberdesque *et al.* on a different oxide glass composition, namely a commercial zinc-phosphate glass from the Argolight company, demonstrating the universality of the Type A WBGs formation process in silver-sensitized glasses. For this purpose, the inscription of helicoidal WBG structures is here reported and their geometrical properties are discussed, unfolding new features. Moreover, modelling based on the Coupled Wave Theory (CWT) is adopted to extract the effective coupling coefficients and lengths of the inscribed WBGs.

Optical Materials EXPRESS

2. Experimental results and discussion

2.1. Glass and direct laser writing

The sample used in this work is a commercial silver-containing zinc-phosphate glass $AG01$ from Argolight company, with nominal cationic composition (mol%) $39.4P_2O_5 - 53.8ZnO - 5.8Ag_2O - 1Ga_2O_3$, which typically corresponds to a 8% cationic fraction of silver elements. The sample motion under femtosecond irradiation was achieved using motorized 3D translation stages (XMS-50) from Newport MKS, assuring sample position within 50 nm precision. The laser used in this work is a KGW:Yb femtosecond oscillator, up to 2.9 W, 9.8 MHz, 390 fs FWHM at 1030 nm, from Amplitude Systems. An AcoustOptics Modulator (AOM) was used to control the pulse energy and a Spatial Light Modulator (SLM) (LCOS, X10468-03, HAMAMATSU Photonics) was used to correct the spherical aberrations after focusing in the glass sample using a high Numerical Aperture (NA) microscope objective (Olympus - 100× NA 1.3), and associated index matching oil (n_{oil} = 1.518).

2.2. Inscription of Type A periodic gratings with periodic Δn

The inscription of WBGs with periods well below the diffraction limit was demonstrated in 2023 in a different glass matrix, namely in a silver-containing sodium-gallo-phosphate glass [23]. In this work, the same approach for the inscription of the Type A WBGs was followed in a commercial silver-containing zinc-phosphate glass to demonstrate the universality of the process. The modulation of the refractive index with sub-wavelength periodicity is assured by the property of TypeA modifications to constantly access the silver reservoir of the glass matrix during consecutive laser scans. [24].

Fig. 1(a) shows the fluorescence images of gratings with different periodicities. Using a microscope objective with NA 0.75, the double track separation is typically 1.6 μm. The spot diameter is thus estimated to ϕ = 1.6 μm, corresponding here to $\phi = 1.16\frac{\lambda}{NA}$, which estimation is close to the Rayleigh criterion. When the grating periodicity Λ is larger than the laser spot diameter, as in the case of the structure shown on the left in Fig. 1(a), the associated refractive index modulation shows the typical double-peak profile of the Type A index modulation (as reported in Fig. 1(c)) that results from the laser-induced silver clusters at the edge of the interaction voxel [21]. The refractive index profile has been extracted from the phase image reported in Fig. 1(b), acquired by phase imaging microscopy with a Sid4BIO camera and software from Phasics company. However, when the grating periodicity Λ becomes smaller than the laser spot diameter, each of the subsequent laser scans achieves two processes, with (i) the photo-dissociation of one of the previously inscribed silver-sustained tracks and (ii) the additional creation of a new double-track structure shifted at a distance Λ, as reported in Fig. 1(a) for examples Λ = 1 μm and 0.5 μm. The refractive index profile for a grating with period Λ = 1 μm, and length L = 25 μm is reported in Fig. 1(d).

2.3. Inscription of Type A periodic gratings supported by helicoidal structures

In this work, Type A WBGs are obtained by inscribing a periodic grating on top of a Type A waveguide. A typical Type A WBG is imaged by fluorescence and phase image microscopy in Figs. 2(a) and 2(b), respectively. It is noteworthy to emphasize that, while the modulation of the refractive index associated with the BGs can not be resolved with considered experimental resolution, it results in a locally averaged Δn value that corresponds to a positive refractive index offset. Indeed, the positive offset from the BG adds up to that of the pre-inscribed index contrast of the waveguide, as shown in Fig. 2(c). Such a refractive index accumulation is assured by the shot-to-shot memory of the Type A modifications, which was demonstrated in the literature and exploited to significantly increase the Type A index contrast [24]. For the particular case of the helicoidal Type A WBGs, the inscription of such structures occurred in two steps. In

Optical Materials EXPRESS

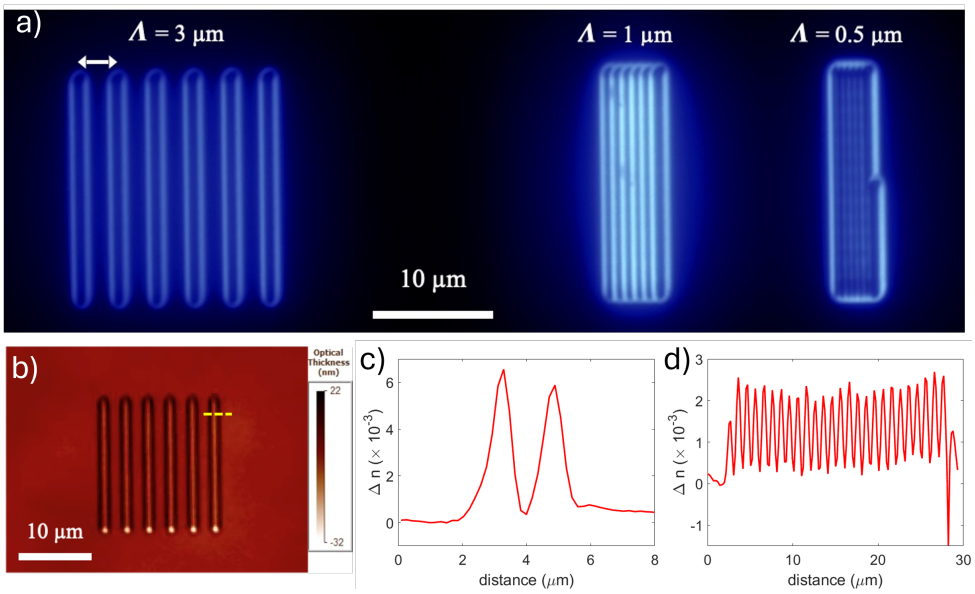

Fig. 1. (a) Fluorescence images of Type A structures with three distinct periodicities with or without laser overlap between successive laser passes (obtained under wide field excitation at λ_{exc} = 375 nm using a 60× microscope objective with NA 0.7). (b) Phase image of the $\Lambda = 3\ \mu m$ period structure showed in (a) obtained using a 100× microscope objective with NA 1.3 and index matching oil with n=1.518. (c) Δn Refractive index profile of the structure in (b) along the yellow dashed line. (d) Δn Refractive index profile of a periodic structure with $\Lambda = 1\ \mu m$ and length $L = 25\ \mu m$, showing the distribution of periodically-spaced refractive index steps after successive laser scans separated by a distance Λ smaller than the beam spot diameter ϕ.

the first step, the waveguide was inscribed at 170 μm below the sample surface, a distance for which the aberrations induced by the focusing objective are minimized. Due to the use of a high numerical aperture (NA 1.3) microscope objective, single-pass Type A waveguides show typical dimensions of the beam spot diameter ϕ = 800 nm for the distance between the two silver-sustained tracks in the plane perpendicular to the propagation direction of the laser beam, *i.e.* the xy plane. Such a 0.8 μm beam size estimation appears very close to usual estimation of $\phi = 1.04\frac{\lambda}{NA}$ that corresponds to the full width at half maximum of the well-known Besse function J_1 of first kind. The associated thickness is 3 μm along the propagation direction of the inscribing laser, *i.e.* the z-axis. Such a 3 μm thickness was measured from the side view of the sample under wide-field white-light microscope imaging (after cutting the sample to intersect the waveguide and then repolishing the lateral face). In the second step, the helicoidal BGs were inscribed by overlapping the guiding structure with a typical length of L=500 μm on the y-axis (axis of sample motion), and with radii of 20 μm and 1.5 μm on the x- and z-axes, respectively. Such an helicoidal trajectory and associated radii corresponds to the trajectory of the center of the laser-glass voxel. At each position along the helix trajectory, the helix track is locally 3 μm thick (similar to the thickness of the waveguide). In this framework, the vertical radius of 1.5 μm of the helix trajectory has been chosen so that the inscribed helix track fully overlaps vertically the 3 μm thickness of the waveguide over one helix period. The helix track even spans vertically 1.5 μm above and below the waveguide section. Choosing such a vertical radius of 1.5 μm for the helix trajectory is expected to allow for the strongest possible WBG, since (i) larger radii would lead to a lower vertical overlap with the waveguide and associated waveguided mode and (ii)

Optical Materials EXPRESS

smaller radii would lead to the partial overwriting of the helix track with itself from one half period to the next one, leading thus to possible detrimental effect over the amplitude of the index modulation. As a result, the Type A waveguide is placed at the center of the ellipse made by the projection of the helicoidal gratings on the xz plane, as shown in Fig. 3(a). As a consequence, during the inscription of a single period Λ_{helix} of the helix, the helicoidal BG intersects the Type A waveguide at the top and at the bottom of the guiding structure, as represented in Fig. 3(b). This results in the inscription of an additional periodicity in the waveguide, such periodicity being equal to half the sought periodicity of the BGs, $\Lambda = \frac{\Lambda_{helix}}{2}$, due to the peculiarity of Type A modifications to build up the associated positive index change during consecutive laser scans. For the sake of clarity, Fig. 3(b) reports a representation of the two-step inscription process of the helicoidal Type A WBGs, while Fig. 5 highlights the two resulting induced periodicities: Λ_{helix} and $\frac{\Lambda_{helix}}{2}$.

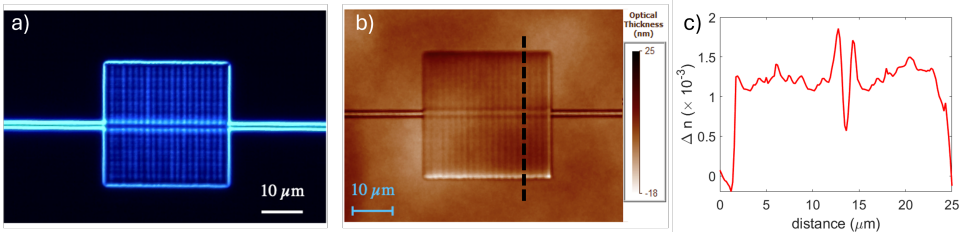

Fig. 2. a) Fluorescence image of a Type A WBG with period $\Lambda = 500$ nm, acquired using a 60× microscope objective with N.A. 0.7, and $\lambda_{exc} = 375$ nm. (b) Phase image of the structure in (a) acquired using a 100× microscope objective with N.A. 1.3 and index matching oil (n=1.518). (c) Δn Refractive index profile along the black dashed line in b), showing the overlapped BG and waveguide's refractive index profiles.

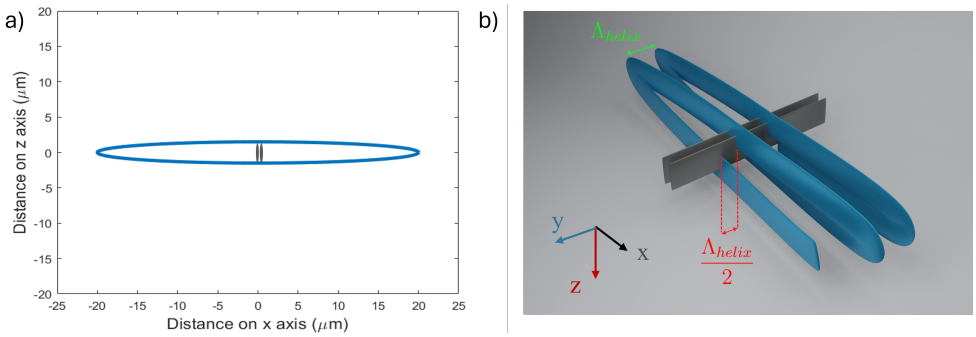

Fig. 3. a) Projection of the helicoidal trajectory that sustains the Type A WBG on the xz plane showing the semi-axis in the two x- and z-axes and the positioning of the Type A waveguide at the center of the ellipse (the 3 μm thickness along the helicoidal track is not shown in (a) but appears clearly in (b)). b) Representation of the two-step inscription of a helicoidal Type A WBG: the helicoidal structure, blue, is inscribed on top of the Type A guiding structure, reported in grey. The overwriting of the helicoidal structure on the waveguide allows for the inscription of two periodicities: the sought periodicity of the helix, Λ_{helix}, and a second equal to its half $\frac{\Lambda_{helix}}{2}$.

Optical Materials EXPRESS

2.4. Transmission and reflection spectra of helicoidal WBGs

The helicoidal Type A WBGs were characterized by transmission and reflection measurements. These spectra were recorded by an Optical Spectrum Analyzer (OSA), AQ6370D with resolution up to 0.02 nm from YOKOGAWA, and processed to discrete only the BGs contribution to the spectra. The inscribed WBGs select Bragg resonances in the NIR range and in the far red range of the visible spectrum, typically in a range λ_B = 780 nm - 1550 nm. A Ti:Sapphire laser, Chameleon Ultra I (Coherent company) with repetition rate 80 MHz, and output power > 2.9 W at 800 nm, has been used to characterize the WBGs in the range 700 nm to 1030 nm. In this case, the WBGs structures were injected in free space using a 20× microscope objective (N.A. 0.5). The output of each waveguide was collected using a 100× microscope objective with N.A. 0.9. The transmission spectra were acquired by focusing the output of each waveguide, selected through a pinhole, on a SM fiber connected to the OSA. The reflection spectra in the range 700 nm - 1030 nm were acquired in free space by inserting a 50-50 beam splitter before the injection objective and by collecting the back-reflected light from the WBG using a 20× microscope objective (with N.A. 0.26) and injecting it into a SM fiber connected to the OSA.

The transmission spectra at the telecommunication wavelength were acquired by injecting the WBGs using a butterfly diode laser SLD1550S-A4 (Thorlabs company), with 40 mW ASE power at 1550 nm. The injection of the source and the collection of light transmitted by the WBGs were achieved by butt-coupling SM fibers to the sample and optimizing the coupling by adopting two 6-axis fiber positioners. Thus, the transmission spectrum of each WBG was acquired by OSA. The reflection spectra were obtained by connecting the butterfly diode to port 1 of a SM circulator, from Thorlabs company, while port 2 was used to inject the sample and port 3 was connected directly to the OSA.

Figure 4 reports the normalized transmission spectra and raw reflection signals at $\lambda_B \sim 1560$ nm for Fig. 4(a), and $\lambda_B \sim 786$ nm for Fig. 4(b), the two WBGs were having different lengths, respectively L = 750 μm and L = 500 μm, but the same helicoidal periodicity Λ_{helix} = 490 nm. These profiles demonstrate the ability of the Type A WBGs to select narrowband resonances and act as mirrors. The effect of polarization upon the WBGs' behavior has been investigated by rotating the orientation of the input linear polarization, which led to no significant dependence on the Bragg resonance properties.

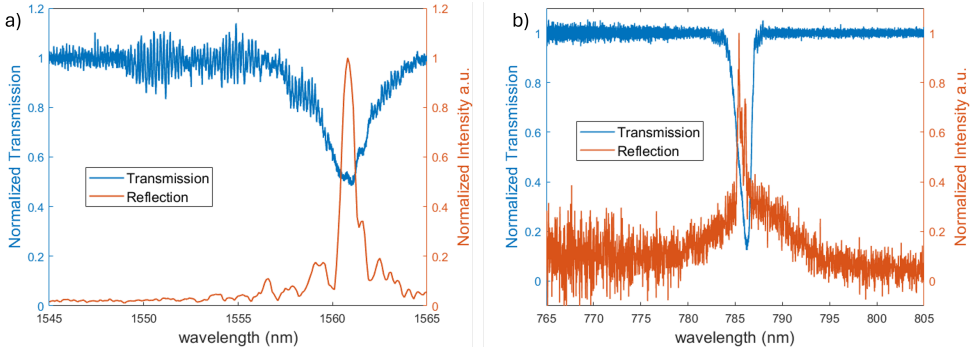

Fig. 4. Reflection and transmission spectra at a) $\lambda_B \sim 1560$ nm and b) $\lambda_B \sim 786$ nm for helicoidal WBGs with Λ_{helix} = 490 nm and lengths a) L = 750 μm and b) L = 500 μm. The reflection spectrum in a) was collected using a SM circulator butt-coupled to the sample, while the reflection spectrum in b) was collected from the back-reflection of the Type A WBGs guided light which was focused on a SM fiber connected to the OSA.

Knowing the refractive index of the glass, $n_g \sim 1.59$, it can be deduced that the Bragg resonance in Fig. 4(a) represents the first-order of diffraction of the helicoidal structure having periodicity

Optical Materials EXPRESS

Λ_{helix} = 490 nm. However, the Bragg resonance reported in Fig. 4(b) can not be considered as second-order diffraction since the drop in transmission ($T_{drop} \sim 88\%$ with L = 500 μm) at the $\lambda_B \sim 786$ nm is considerably greater than what is achieved at the first-order ($T_{drop} \sim 50\%$ with L = 750 μm) at the $\lambda_B \sim 1560$ nm. Eventual data points above 1 for normalized transmission spectra and below zero in reflected signals shall be considered as experimental noise as they result from the management of the reference spectra and/or the background signals.

The improved diffraction efficiency can be explained by recalling the Direct Laser Writing (DLW) fabrication process of the helicoidal gratings, reported in Fig. 3(b), which leads to the inscription of two periodic structures, one having the periodicity of the helix, Λ_{helix}, the other having periodicity $\frac{\Lambda_{helix}}{2}$. Such a periodic grating is associated with a modulation of the refractive index with a period $\frac{\Lambda_{helix}}{2}$, which introduces a non-zero-Fourier component at $\lambda_B = 2n_{eff}\Lambda_{helix}/2$, as measured in Figs. 4(b) and 6, and as illustrated by Fig. 5. Moreover, Fig. 5 shows the cases of two modes guided in a Type A WBG with a helix period Λ_{helix} and induced smaller periodicity $\frac{\Lambda_{helix}}{2}$. As illustrated in the schematic representation, a more confined mode is mostly affected by the coupling with the smaller periodicity $\frac{\Lambda_{helix}}{2}$, while a mode more extended in the plane perpendicular to the propagation direction will evanescently couple the BG having periodicity Λ_{helix}.

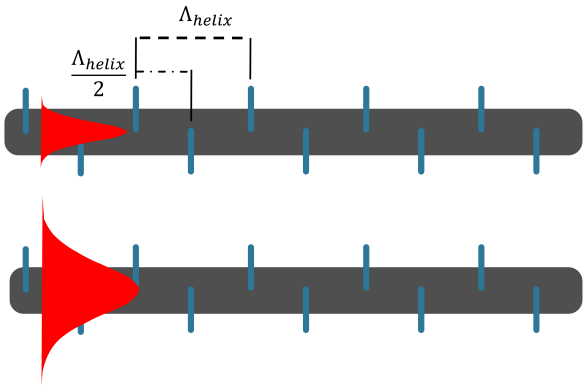

Fig. 5. Schematic representation of the projection of the helicoidal WBG on a zy plane: this allows to easily retrieve the two periodicities, Λ_{helix} and $\frac{\Lambda_{helix}}{2}$, induced during the inscription of a single period of the helicoidal structure. Moreover, it allows for comparing the evanescent coupling with the two periodicities for the cases of more-confined (top), and less-confined (bottom) guided modes.

Figure 6 provides evident support to the double-periodicity hypothesis: the blue curve reported demonstrates a T_{drop}>99% drop in transmission at the Bragg resonance $\lambda_B \sim 1007$ nm for a helicoidal Type A WBGs having Λ_{helix} = 630 nm and length L = 500 μm, excluding the chance of second order diffraction.

CWT-based modelling allowed for retrieving the coupling coefficient κ and the effective length L_{eff} of the WBGs reported in Fig. 6. The numerical solution for the reflection coefficient ρ of the Type A WBG

$$\rho = \frac{-\delta + i\sqrt{(\kappa-\delta)(\kappa+\delta)}\, tanh\left[L_{eff}\sqrt{(\kappa-\delta)(\kappa+\delta)} - i\, arctanh\left(\frac{\delta}{\sqrt{\kappa^2-\delta^2}}\right)\right]}{\kappa}, \tag{2}$$

is a function of the coupling coefficient κ, the effective length L_{eff}, and the detuning from the resonance condition $\delta = 2\pi(\frac{1}{\lambda} - \frac{(2n_{eff})}{\Lambda_G})$, where Λ_G is the period of the gratings, and has been

Optical Materials EXPRESS

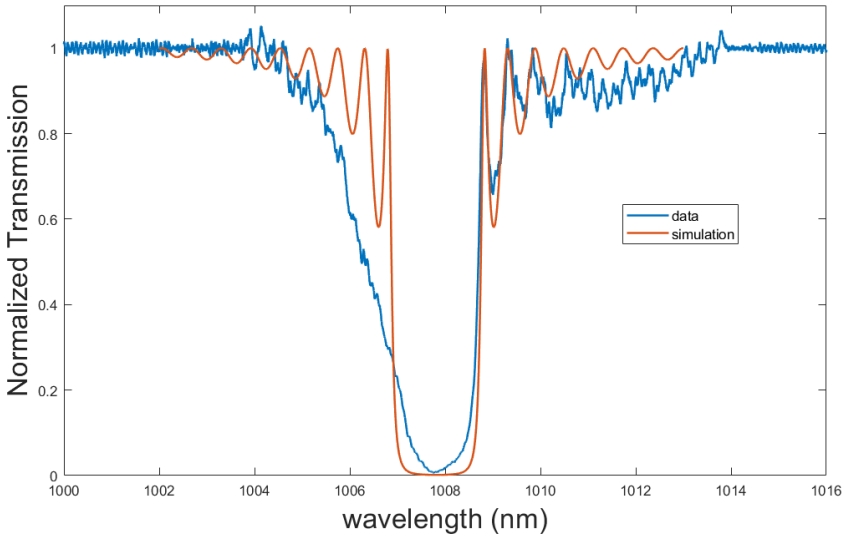

Fig. 6. Transmission spectrum, in blue, of a helicoidal Type A WBG having Λ_{helix} = 630 nm and length L = 500 μm. The Bragg resonance at λ_B ~1007 nm shows a drop in transmission T_{drop}>99%. A CWT-based modeling allowed for retrieving the effective parameters of the simulated WBG, in orange.

obtained by Mathematica software by resolving the Kogelnik problem [28]

$$\frac{dR}{dz} = i\sigma\, R(z) + i\kappa\, S(z), \tag{3a}$$

$$\frac{dS}{dz} = -i\sigma\, S(z) - i\kappa * R(z), \tag{3b}$$

for the forward $R(z) \equiv A(z)exp(i\delta z - \phi/2)$ and backward $S(z) \equiv B(z)exp(i\delta z + \phi/2)$ waves propagating in the dielectric waveguide. Here, $\phi(z)$ represents an eventual chirp of the gratings. The solution reported in Eq. (2) represents a general solution to the CWT problem with the boundary conditions

$$R(-L/2) = 1, \tag{4a}$$

$$S(L/2) = 0, \tag{4b}$$

as reported in Kogelnik's work, and no further assumption has been made. Using Eq. (2), it was possible to retrieve the effective length L_{eff} = 498 μm and the coupling coefficient κ_{sim} =7.85 mm^{-1} for the Type A WBG reported in Fig. 6. The width between the two first zeros of the fitted response $\Delta\lambda_{fit}$= 2.1 nm from Eq. (2) corresponds quite well to the experimental bandwidth (full width at half maximum) $\Delta\lambda_{exp}$= 2.6 nm. By comparison with the results reported in the literature, it is clear that Type A WBGs show a strong coupling coefficient: for instance, it is more than one order of magnitude higher than what is reported in the work of Ams *et al.* for a 4 mm long WBG in a silicate glass (κ_{silic}=0.634 mm^{-1} at λ_B=1030 nm) [11].

However, the theoretical bandwidth of the Bragg resonance for such an efficient WBG can be calculated also by [11]

$$\Delta\lambda = \frac{\lambda_B^2}{n_{eff}}\sqrt{\frac{\kappa_{sim}^2}{\pi^2} + \frac{1}{L_{eff}^2}} \tag{5}$$

leading to an estimation of $\Delta\lambda$ = 1.3 nm, which is two times smaller than the experimental result. Moreover, the experimental transmission curve reported in Fig. 6 is not symmetric, contrarily to

Optical Materials EXPRESS

what a priori expected. Therefore, it may be assumed that a chirp has been induced during the inscription process of the periodic helicoidal structure.

2.5. Adapted waveguides and helicoidal WBGs

It gets clear that the accuracy of sample positioning during the whole DLW process of the WBG is a nontrivial parameter to take into consideration: indeed, it requires maintaining the absolute positioning precision better than a fraction of the targeted periodicity over hundreds or even thousands of WBG periods. Moreover, a misalignment between the waveguide and the centre of the helicoidal gratings can affect not only the position of the λ_B but also the strength of the resonance. Therefore, to account for this issue, the Type A waveguides have been engineered by adopting the multiscan technique already discussed in the work of Loi *et al* [24]. Engineered square-based waveguides have been inscribed by a series of 16 consecutive laser scans with 125 nm between each line to obtain a square-like structure of 3 $\mu m\times$ 3 μm as shown in Fig. 7(a). The produced waveguide showed a single-mode behavior under propagation at 1030 nm, as shown in Fig. 7(b), since the output waveguided profile remained the same whatever the injection conditions (only the amplitude was varying then, due to modifications of the injection efficiency). The multi-scan approach has allowed thus to adapt the waveguide profile to a Gaussian-like geometry leading to better injection coupling coefficients. Lineic losses are not addressed in the present investigation as it had been previously discussed in detail [24], leading to an average loss of 0.34±0.06 dB/cm in this glass in the 750-1030 nm spectral range which encompasses single and multi-pass approaches. Moreover, the insertion losses of the WBGs typically correspond to an overall attenuation by a factor 2 or 3 of the output guided light collected at the end of the WG, depending on the WBG inscription conditions. Since the WBG behaves as a kind of planar waveguide itself, it introduces a mode mismatch of the guided mode at the entrance of the WBG which leads to modal losses and partial light decoupling. Propagation losses over the 500 μm length of the WBGs are negligible compared to decoupling losses. Limiting these modal decoupling would require limiting the strength of the grating (with lower WBG laser inscription conditions upon the pre-inscribed WG) and/or apodizing the WBG profile, so as to achieve adiabatic coupling of the guided mode to the mode profile inside the WBG: these aspects are beyond the scope of the present demonstration of high-contrast Type A WBGs. The helicoidal Type A grating is then inscribed on top of the engineered waveguide following the above-mentioned procedure, with Λ_{helix} = 648 nm resulting in an effective period $\frac{\Lambda_{helix}}{2}$ = 324 nm for the propagating mode. Nevertheless, such a wide waveguide allows for strong improvement in the overlap between the guided mode propagating in the waveguide and BGs structure. To demonstrate both the efficiency of the Bragg resonance and the repeatability of the inscription process, several engineered Type A WBGs were inscribed with different lengths. Figure 8 shows the evolution of the experimental transmission drop as a function of the length of the helicoidal Type A gratings.

For the series of WBGs, a mean coupling coefficient κ_{mean} has been extracted by fitting the experimental data using the following equation:

$$1 - R_{max} = 1 - tanh^2(\kappa L), \tag{6}$$

leading to obtain κ_{mean} = 5.00 ± 0.15 mm^{-1} at λ_B = 1035 ± 0.5 nm.

Moreover, data reported in Fig. 8 for the engineered WBGs series show a quick enhancement of the BGs performance for gratings lengths from 200 μm to 400 μm and a stabilization of the experimental reflectivity around 97% for Bragg gratings having lengths greater than 500 μm. Indeed, the highest experimental reflectivity has been achieved by WBGs having 500 μm long BG, with more than 99.7% drop in transmission at 1035.4 nm and a resonance bandwidth of 1.4 nm, which is 1.86 times smaller than what is achieved by single pass helicoidal Type A WBGs.

Optical Materials EXPRESS

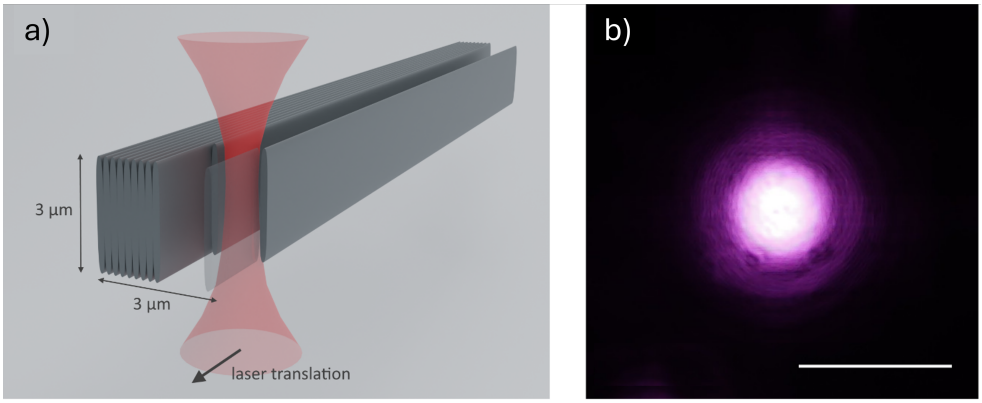

Fig. 7. a) Sketch of the multi-scan square-like waveguide of 3 μm× 3 μm. b) Near-field image of the waveguide output guided mode at 1030 nm (scale bar = 10 µm).

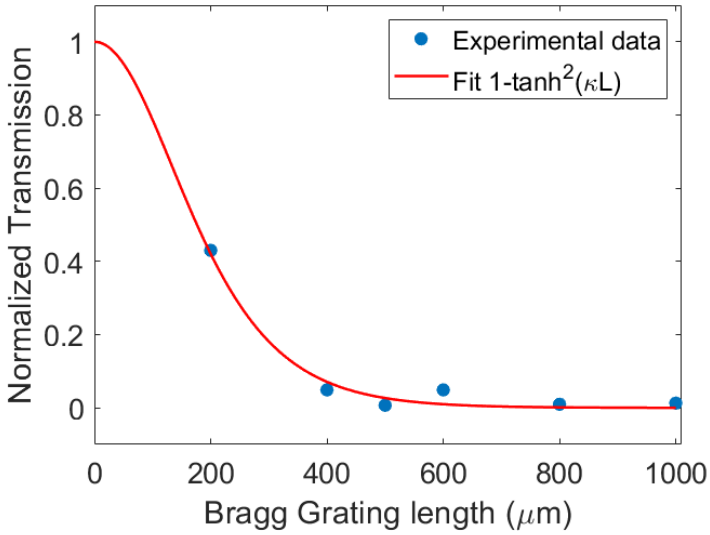

Fig. 8. Experimental transmission at 1035 nm (Bragg resonance) of different WBG for lengths ranging from 200 μm to 1 mm (blue points) and the best fit of Eq. (6) with κ_{mean}=5mm^{-1}.

3. Conclusions

This work reports on the fabrication of efficient first-order Type A WBGs in a commercial silver-containing glass for applications in the NIR range. Due to the rewriting property of Type A modifications, Type A WBGs were realized with periodicities well below the diffraction limit, with effective periodicities down to 245 nm, being always associated with a positive modulation of the refractive index of the glass having the same period. Transmission and reflection spectra of the inscribed Type A WBGs show the abilities of the silver-sustained structures to act as narrowband mirrors.

Moreover, it has been demonstrated that the fabrication of helicoidal Type A WBGs can induce the simultaneous inscription of two periodicities: one given by the helix period Λ_{helix}, the other given by half the helix period $\frac{\Lambda_{helix}}{2}$. Such a remarkable result has been exploited for the fabrication of efficient first-order WBGs in the far-red visible and NIR ranges. Finally,

Optical Materials EXPRESS

numerical simulations based on Kogelnik's CWT model allowed for retrieving remarkably high coupling coefficients in the NIR, more than an order of magnitude higher than what has been reported in the literature. Additionally, a moderate asymmetrical transmission curve suggests the presence of a chirp in the inscribed period, which resulted also in the broadening of the Bragg resonance bandwidth. Such a chirp could be attributed to instabilities during the DLW process that consequently affect the effective length of the gratings by shortening it. In this regard, an interesting perspective would take into consideration the inscription of silver-sustained gratings by phase mask approach.

Nevertheless, engineered Type A WBGs have been proposed in this work to account for the nontrivial positioning issue. The series of helical WBGs with increasing grating length has demonstrated the repeatability of the DLW inscription process and highlighted the fact that the optimum efficiency of type A WBGs is achieved at a short grating length of 500 μm thanks to the very high coupling coefficient κ.

In conclusion, this work has demonstrated that Type A modifications can be exploited for the fabrication of efficient optical devices, paving the way for highly compact WBGs and for more complex architectures such as Fabry-Perot cavities.

Funding. Grand Research Program « LIGHT » Idex University of Bordeaux; Marie Skłodowska-Curie (823941); Region Nouvelle Aquitaine (APPR2020-2019-8193110]); Agence Nationale de la Recherche (ANR-19- CE08-0021).

Acknowledgements. This research was funded by French National Research Agency (ANR) [Grant: ANR-19-CE08-0021] and Region Nouvelle Aquitaine [Grant: APPR2020-2019-8193110], from European Union's Horizon 2020 research & innovation program under the Marie Skłodowska-Curie grant agreement No 823941, from the Grand Research Program ≪ LIGHT ≫ Idex University of Bordeaux, and from the Graduate program ≪ EUR Light S&T≫ PIA3 ANR-17-EURE-0027.

Disclosures. The authors declare no conflicts of interest.

Data Availability. Data underlying the results presented in this paper are not publicly available at this time but may be obtained from the authors upon reasonable request.

References

1. R. Kashyap, *Fiber Bragg Gratings*, Electronics & Electrical (Elsevier Science, 1999).
2. G. Meltz, W. W. Morey, and W. H. Glenn, "Formation of bragg gratings in optical fibers by a transverse holographic method," Opt. Lett. **14**(15), 823–825 (1989).
3. K. O. Hill, B. Malo, F. Bilodeau, *et al.*, "Bragg gratings fabricated in monomode photosensitive optical fiber by uv exposure through a phase mask," Appl. Phys. Lett. **62**(10), 1035–1037 (1993).
4. K. Byron, K. Sugden, T. Bricheno, *et al.*, "Fabrication of chirped bragg gratings in photosensitive fibre," Electron. Lett. **29**(18), 1659–1660 (1993).
5. D. V. Przhiialkovskii and O. V. Butov, "High-precision point-by-point fiber bragg grating inscription," Results Phys. **30**, 104902 (2021).
6. G. D. Marshall, M. Ams, and M. J. Withford, "Direct laser written waveguide-bragg gratings in bulk fused silica," Opt. Lett. **31**(18), 2690–2691 (2006).
7. H. Zhang, S. M. Eaton, and P. R. Herman, "Single-step writing of bragg grating waveguides in fused silica with an externally modulated femtosecond fiber laser," Opt. Lett. **32**(17), 2559–2561 (2007).
8. G. D. Marshall, R. J. Williams, N. Jovanovic, *et al.*, "Point-by-point written fiber-bragg gratings and their application in complex grating designs," Opt. Express **18**(19), 19844–19859 (2010).
9. J. Burgmeier, C. Waltermann, G. Flachenecker, *et al.*, "Point-by-point inscription of phase-shifted fiber bragg gratings with electro-optic amplitude modulated femtosecond laser pulses," Opt. Lett. **39**(3), 540–543 (2014).
10. S. Antipov, M. Ams, R. J. Williams, *et al.*, "Direct infrared femtosecond laser inscription of chirped fiber bragg gratings," Opt. Express **24**(1), 30–40 (2016).
11. M. Ams, P. Dekker, S. Gross, *et al.*, "Fabricating waveguide bragg gratings (wbgs) in bulk materials using ultrashort laser pulses," Nanophotonics **6**(5), 743–763 (2017).
12. N. Jovanovic, J. Thomas, R. J. Williams, *et al.*, "Polarization-dependent effects in point-by-point fiber bragg gratings enable simple, linearly polarized fiber lasers," Opt. Express **17**(8), 6082–6095 (2009).
13. C. Miese, M. J. Withford, and A. Fuerbach, "Femtosecond laser direct-writing of waveguide bragg gratings in a quasi cumulative heating regime," Opt. Express **19**(20), 19542–19550 (2011).
14. K. Hirao and K. Miura, "Writing waveguides and gratings in silica and related materials by a femtosecond laser," J. Non-Cryst. Solids **239**(1-3), 91–95 (1998).
15. J. W. Chan, T. Huser, S. Risbud, *et al.*, "Structural changes in fused silica after exposure to focused femtosecond laser pulses," Opt. Lett. **26**(21), 1726–1728 (2001).

Optical Materials EXPRESS

16. A. M. Streltsov and N. F. Borrelli, "Study of femtosecond-laser-written waveguides in glasses," J. Opt. Soc. Am. B **19**(10), 2496–2504 (2002).
17. M. Lancry, B. Poumellec, A. Chahid-Erraji, *et al.*, "Dependence of the femtosecond laser refractive index change thresholds on the chemical composition of doped-silica glasses," Opt. Mater. Express **1**(4), 711–723 (2011).
18. B. Poumellec, M. Lancry, A. Chahid-Erraji, *et al.*, "Modification thresholds in femtosecond laser processing of pure silica: review of dependencies on laser parameters," Opt. Mater. Express **1**(4), 766–782 (2011).
19. A. A. Khalil, J. Bérubé, S. Danto, *et al.*, "Direct laser writing of a new type of waveguides in silver containing glasses," Sci. Rep. **7**, 2045–2322 (2017).
20. Y. Petit, S. Danto, T. Guérineau, *et al.*, "On the femtosecond laser-induced photochemistry in silver-containing oxide glasses: mechanisms, related optical and physico-chemical properties, and technological applications," Adv. Opt. Technol. **7**(5), 291–309 (2018).
21. M. Bellec, A. Royon, B. Bousquet, *et al.*, "Beat the diffraction limit in 3d direct laser writing in photosensitive glass," Opt. Express **17**(12), 10304–10318 (2009).
22. A. A. Khalil, J.-P. Bérubé, S. Danto, *et al.*, "Comparative study between the standard type i and the type a femtosecond laser induced refractive index change in silver containing glasses," Opt. Mater. Express **9**(6), 2640–2651 (2019).
23. R. Laberdesque, L. Loi, T. Guérineau, *et al.*, "Three-dimensional femtosecond laser inscription of type a-based high-efficiency first-order waveguide bragg gratings," Adv. Opt. Technol. **12**, 1 (2023).
24. L. Loi, Y. Petit, and L. Canioni, "High refractive index change in type a laser modification using a multi-scan approach," Opt. Mater. Express **12**(6), 2297–2308 (2022).
25. E. Smetanina, B. Chimier, Y. Petit, *et al.*, "Modeling of cluster organization in metal-doped oxide glasses irradiated by a train of femtosecond laser pulses," Phys. Rev. A **93**(1), 013846 (2016).
26. T. de Castro, A. A. K. H. Fares, R. Laberdesque, *et al.*, "Modeling of cluster organization in metal-doped oxide glasses irradiated by a train of femtosecond laser pulses," J. Non-Cryst. Solids **517**, 51-56 (2019).
27. D. Tan, P. Jiang, B. Xu, *et al.*, "Modeling of cluster organization in metal-doped oxide glasses irradiated by a train of femtosecond laser pulses," Adv. Photonics Res. **2**(4), 2000121 (2021).
28. H. Kogelnik, *Theory of Dielectric Waveguides* (Springer Berlin Heidelberg, 1975), pp. 13–81.